Effect of Thermal Creep on Heat Transfer for a Two-Dimensional Microchannel Flow: An Analytical Approach

Barbaros Çetin
Mechanical Engineering Department,
Microfluidics & Lab-on-a-Chip Research Group,
Ihsan Dogramaci Bilkent University,
Ankara 06800, Turkey
e-mails: barbaros.cetin@bilkent.edu.tr,
barbaroscetin@gmail.com

In this paper, velocity profile, temperature profile, and the corresponding Poiseuille and Nusselt numbers for a flow in a microtube and in a slit-channel are derived analytically with an isoflux thermal boundary condition. The flow is assumed to be hydrodynamically and thermally fully developed. The effects of rarefaction, viscous dissipation, axial conduction are included in the analysis. For the implementation of the rarefaction effect, two different second-order slip models (Karniadakis and Deissler model) are used for the slip-flow and temperature-jump boundary conditions together with the thermal creep at the wall. The effect of the thermal creep on the Poiseuille and Nusselt numbers are discussed. The results of the present study are important (i) to gain the fundamental understanding of the effect of thermal creep on convective heat transfer characteristics of a microchannel fluid flow and (ii) for the optimum design of thermal systems which includes convective heat transfer in a microchannel especially operating at low Reynolds numbers. [DOI: 10.1115/1.4024504]

Keywords: microchannel, Knudsen number, second-order slip model, thermal creep

1 Introduction

With the today's fabrication facility, fabrications of channels with a size in the order of micrometers are not an issue (even the fabrication of microtubes with the diameters of several micrometers/nanometers have become possible [1]). These kinds of small channels can easily be the elements of microheat exchangers, microheat sinks, microsensors, and micropower generation systems. For an effective and economical design of microfluidic systems, heat transfer characteristics of flow inside these microchannels need to be well understood. Although, there exists some experimental data for fluid flow [2–4], experimental data on convective heat transfer for single phase microchannel flow are very restricted [5]. Yet, numerical and analytical models with an appropriate slip model are a key ingredient for the analysis of fluid flow and heat transfer in a microchannel.

As the characteristic length (L) of the flow approaches to the mean-free-path (λ) of the fluid, the continuum approach fails to be valid, and the fluid flow modeling moves from continuum to molecular model. The ratio of the mean-free-path to the characteristic length of the flow (L) is known as the Knudsen number ($\mathrm{Kn} = \lambda/L$). For the Kn number varying between 0.01 and 0.1 (which corresponds to the flow of the air at standard atmospheric conditions through the channel that has the characteristic length of $0.7 \sim 7\ \mu$m), the regime is known as the slip-flow regime. In this regime, flow can be modeled with the continuum modeling as far as the boundary conditions are modified to take into account the rarefaction effects.

For Kn number between 0.1 and 10, the regime is known as transition regime. In this regime, the Navier–Stokes fails to model the fluid flow, and a molecular model is necessary. Either molecular simulations like direct simulation of Monte Carlo (DSMC) and MD or solutions of Boltzmann transport equation which require appreciable computational effort are required. However, one preferable alternative to extend the applicability of Navier–Stokes equations into the transition regime is to introduce second-order slip models. Although strictly speaking Navier–Stokes equations are valid Kn number up to 0.1, several studies [2,3,6] indicated that Navier–Stokes equations with second-order slip models can predict the fluid flow behavior up to $\mathrm{Kn} \approx 0.25$.

The general form of the boundary conditions for velocity and temperature can be written as follows:

$$u - u_w = a_1 \lambda \left(\frac{\partial u}{\partial n}\right)_w + a_2 \lambda^2 \left(\frac{\partial^2 u}{\partial n^2}\right)_w + a_3 \lambda^2 \left(\frac{\partial T}{\partial t}\right)_w \quad (1)$$

$$T - T_w = b_1 \lambda \left(\frac{\partial T}{\partial n}\right)_w + b_2 \lambda^2 \left(\frac{\partial^2 T}{\partial n^2}\right)_w \quad (2)$$

where n, t, and w stand for normal direction, tangential direction, and channel wall, respectively. First term of Eqs. (1) and (2) are known as the first-order boundary conditions and used as first-order slip model [7]. The second terms are known as the second-order boundary conditions and used as second-order slip model [7]. There exists many different second-order models with different coefficients [3,8]; however, only two of these methods [7,9] have a complimentary second-order temperature boundary condition (the coefficients for the two second-order models are tabulated in Table 1). The last term of the Eq. (1) is known as the thermal creep. Thermal creep (thermal transpiration) is a well-known phenomenon which is observed for rarefied fluids and flow in micro and nanochannels. Basically, thermal creep is the fluid flow in the direction from cold to hot due to the tangential temperature gradient along the channel walls. Thermal creep can enhance or reduce the flowrate in a channel depending on the direction of the tangential temperature gradient at the channel wall. Actually, thermal creep is the basic driving mechanism for Knudsen compressors [7].

In addition to slip-flow, temperature jump and thermal creep, there are some more additional effects associated with the scale of the microchannels. The effect of the viscous dissipation, which is characterized by Brinkman number, and the axial conduction, which is characterized by Peclet number, are negligible at

Contributed by the Heat Transfer Division of ASME for publication in the Journal of Heat Transfer. Manuscript received July 13, 2012; final manuscript received November 15, 2012; published online September 11, 2013. Assoc. Editor: Sushanta K. Mitra.

Table 1 List of the coefficients used in Eqs. (1) and (2)

	a_1	a_2	a_3	b_1	b_2
Karniadakis et al. [6]	1.0	0.5	$\frac{3}{2\pi}\frac{\gamma-1}{\gamma}\frac{c_p\rho}{\mu}$	$\frac{2-F_T}{F_T}\frac{2\gamma}{\gamma+1}\frac{1}{\Pr}$	$\frac{2-F_T}{F_T}\frac{\gamma}{\gamma+1}\frac{1}{\Pr}$
Deissler [7]	1.0	–9/8	$\frac{3}{2\pi}\frac{\gamma-1}{\gamma}\frac{c_p\rho}{\mu}$	$\frac{2-F_T}{F_T}\frac{2\gamma}{\gamma+1}\frac{1}{\Pr}$	$-\frac{9}{128}\frac{177\gamma-145}{\gamma+1}$

macrochannels, and important at microscale [10]. These additional effects result in unconventional heat transfer behavior in microchannels, such as the dependence of the Nusselt number on Reynolds number (for constant wall temperature thermal boundary condition).

Strictly speaking, incompressible model together with slip models is inconsistent [6]; however, many researchers used incompressible flow model to explore the fundamental aspects of the convective heat transfer inside microchannels [2,6,10,11,13–29]. The fluid flow and heat transfer inside a microconduit was analyzed for different geometries, such as circular tube [10,14–21,29], parallel plate (i.e., slit-channel) [18,22–26,30], rectangular channel [2,11–13,27], annular channel [28] using first-order [10,12–14,16–18,22–24,26,28] and second-order models [2,11,19–21,25,27,29,30]. Some studies included the viscous dissipation [10,15–18,20,21,23,24,27] and the axial conduction [12,13,17,18,20,21,23,27]. Very few numerical studies include the effect of the thermal creep on heat transfer [12,13,21,25–27,30] (although, the thermal creep was included in the model [27,30], the slip velocity due to the thermal creep is introduced as a constant u_c instead of function of temperature gradient at the wall).

In this study, velocity profile, temperature profile, and corresponding Poiseuille and Nusselt number expressions are determined for a fully developed gaseous flow in a 2D microchannel (i.e., both microtube and slit-channel) with a constant wall heat flux thermal boundary condition. The flow assumed to be incompressible,[1] laminar, hydrodynamically and thermally fully developed. The thermophysical properties of the fluid are assumed to be constant. Second-order slip model together with the thermal creep term is implemented. Two second-order models, Karniadakis model [6] (**M1** hereafter) and Deissler model [7] (**M2** hereafter) are used. The effect of viscous dissipation, axial conduction is also included in the analysis. Neat, closed form solutions for the fully developed velocity profile, temperature profile, Poiseuille number and Nusselt number are derived analytically. The results of the present study are important (i) to gain the fundamental understanding of the effect of thermal creep on convective heat transfer characteristics of a microchannel fluid flow and (ii) for the optimum design of thermal systems which includes convective heat transfer in a microchannel especially operating at low Reynolds numbers.

2 Analysis

The steady-state, hydrodynamically developed flow with a constant temperature, T_i, flows into a 2-D microchannel with the constant heat flux at the wall. Following dimensionless parameters are used in the analysis:

$$\eta=\frac{2^{2-k}y}{D_h},\quad \xi=\frac{x}{\mathrm{Pe}\cdot D_h/2^{2-k}},\quad \theta=\frac{T-T_i}{\dot{q}''D_h/(2^{2-k}k)},\quad \bar{u}=\frac{u}{u_o}$$
$$u_o=-\frac{dP}{dx}\frac{D_h^2}{4^{3-k}\mu},\quad \mathrm{Pe}=u_oD_h/\alpha,\quad \mathrm{Br}=\frac{2^{2-k}\mu u_o^2}{\dot{q}''D_h} \tag{3}$$

where $k=0$ is for slit-channel and $k=1$ is for microtube (y-coordinate is r for microtube). The channel height is $2H$, and D_h is $4H$ for slit-channel. Both the channel height and D_h are D for microtube. The governing energy equation, including the axial conduction and the viscous dissipation term, and the corresponding boundary conditions can be written as

$$\frac{\bar{u}}{2^{2-k}}\frac{\partial\theta}{\partial\xi}=\frac{1}{\eta^k}\frac{\partial}{\partial\eta}\left(\eta^k\frac{\partial\theta}{\partial\eta}\right)+\frac{1}{\mathrm{Pe}^2}\frac{\partial^2\theta}{\partial\xi^2}+2^{2-k}\mathrm{Br}\left(\frac{\partial\bar{u}}{\partial\eta}\right)^2 \tag{4}$$

$$\begin{aligned}&\theta=0 && \text{at} && \xi=0\\ &\theta\to\theta_\infty && \text{as} && \xi\to\infty\\ &\theta\to\text{finite} && \text{at} && \eta=0\\ &\frac{\partial\theta}{\partial\eta}=1 && \text{at} && \eta=1\end{aligned} \tag{5}$$

where $\bar{u}$ is the dimensionless fully developed velocity profile for the slip-flow regime. By solving the momentum equation together with the slip velocity boundary condition, $\bar{u}$ can be determined as follows:

$$\bar{u}=\frac{u}{u_o}=\chi-\eta^2+\kappa T_\xi \tag{6}$$

where χ and κ are defined as

$$\chi=1+4a_1\mathrm{Kn}-8a_2\mathrm{Kn}^2,\quad \kappa=\frac{3}{2^{1-k}\pi}\frac{\gamma-1}{\gamma}\frac{\mathrm{Kn}^2}{\mathrm{Br}} \tag{7}$$

T_ξ in Eq. (6) represents the temperature gradient at the wall $(\partial\theta/\partial\xi)_{\text{wall}}$ which is unknown prior to the solution of the energy equation.

By using the definition of the friction factor

$$f\equiv\frac{-4\mu(du/dy)_{y=H}}{1/2\rho u_{\text{mean}}^2} \tag{8}$$

Poiseuille number can be determined as

$$\mathrm{Po}=f\cdot\mathrm{Re}=16(2^{2-k})\Omega=\frac{16(2^{2-k})}{\chi-1/(3-k)+\kappa T_\xi} \tag{9}$$

The fully developed temperature profile has the following functional form [6]:

$$\theta_\infty=T_\xi\xi+\phi(\eta) \tag{10}$$

By using the fact that the temperature is fully developed, T_ξ is read as constant. Substituting Eq. (10) into Eq. (4), and integrating once in η-direction results in

$$\frac{d\phi}{d\eta}=\frac{1}{\eta^k}\int\left(\frac{\bar{u}T_\xi}{2^{2-k}}-2^{4-k}\mathrm{Br}\eta^2\right)\eta^k d\eta \tag{11}$$

Using the boundary condition at the wall, the unknown temperature gradient at the wall, T_ξ, can be determined as

$$T_\xi=\frac{\beta+\sqrt{\beta^2+16(3+k)\kappa(2^{2-k}\mathrm{Br}+3-2k)}}{2(3-k)\kappa} \tag{12}$$

[1]The incompressible flow assumption requires Mach number is less than 0.3.

where $\beta = 1-(3-k)\chi$. Integrating Eq. (11) in η-direction and applying the boundary condition at the microchannel center, ϕ can be determined as follows:

$$\phi(\eta) = \frac{\Gamma}{8}\eta^2 - \left(\mathrm{Br} + \frac{T_\xi}{16}\right)\frac{\eta^4}{3-k} + C \tag{13}$$

where C is an arbitrary constant, and $\Gamma = T_\xi(\chi + \kappa T_\xi)$. C can be determined by substituting Eq. (10) into Eq. (4) and integrating the resulting equation in η-direction from 0 to 1, and in ξ-direction as

$$C = \begin{cases} \frac{1}{15}\left(\mathrm{Br}+\frac{T_\xi}{16}\right) - \frac{\Gamma}{24} + \frac{\Omega}{3}\left(\frac{12T_\xi}{\mathrm{Pe}^2} - \frac{8\mathrm{Br}}{105} + \frac{\Gamma}{30} - \frac{T_\xi}{210}\right) & \text{for } k=0 \\ \frac{1}{6}\left(\mathrm{Br}+\frac{T_\xi}{16}\right) - \frac{\Gamma}{16} + \frac{\Omega}{3}\left(\frac{6T_\xi}{\mathrm{Pe}^2} - \frac{\mathrm{Br}}{8} + \frac{\Gamma}{32} - \frac{T_\xi}{128}\right) & \text{for } k=1 \end{cases} \tag{14}$$

Fully developed temperature can be obtained by substituting Eq. (13) into Eq. (10), where constant T_ξ and C are defined in Eqs. (12) and (14), respectively. Note that, to recover the result for the case without thermal creep (i.e., $a_3 \to 0$), the limit of T_ξ needs to be determined. Taking the limit leads to

$$\lim_{a_3 \to 0} T_\xi = -\frac{2^{2+k}(2^{2-k}\mathrm{Br} + 3 - 2k)}{\beta} \tag{15}$$

Using this fact, macrochannel and macrotube [31] results (i.e., $\mathrm{Kn} = \mathrm{Br} = 0$) can be recovered as[2]

$$\theta_\infty = \begin{cases} 6\xi + \frac{3\eta^2}{4} - \frac{\eta^4}{8} - \frac{39}{280} + \frac{36}{\mathrm{Pe}^2} & \text{for } k=0 \\ 8\xi + \eta^2 - \frac{\eta^4}{4} - \frac{7}{24} + \frac{32}{\mathrm{Pe}^2} & \text{for } k=1 \end{cases} \tag{16}$$

Introducing dimensionless quantities, fully developed Nusselt number can be written as

$$\mathrm{Nu}_\infty \equiv \frac{h_\infty D}{k} = -\frac{2^{2-k}}{\theta_\mathrm{m} - \theta_\mathrm{w}} \tag{17}$$

where θ_m is the dimensionless mean temperature

$$\theta_\mathrm{m} = \frac{2^k u_o}{u_\mathrm{m}} \int_0^1 \bar{u}\theta\eta^k d\eta \tag{18}$$

and θ_w is the wall temperature. θ_w can be determined by the implementation of the temperature-jump boundary condition, Eq. (2) as

$$\theta_\mathrm{w} = \theta_\infty(\xi, 1) + 2b_1\mathrm{Kn}\left(\frac{\partial\theta}{\partial\eta}\right)_\mathrm{w} - 4b_2\mathrm{Kn}^2\left(\frac{\partial^2\theta}{\partial\eta^2}\right)_\mathrm{w} \tag{19}$$

Fully developed Nusselt number can be determined as

$$\mathrm{Nu}_\infty = -\frac{2^{2-k}}{\frac{1}{3-k}\left(\mathrm{Br}+\frac{T_\xi}{16}\right) - \frac{\Gamma}{8} - C + \Omega\Upsilon - 2b_1\mathrm{Kn} - 4b_2\mathrm{Kn}^2\left(2(2+k)\mathrm{Br} + \frac{(2k+1)T_\xi}{2^{2+k}} - \frac{\Gamma}{4}\right)} \tag{20}$$

where Υ is defined as

$$\Upsilon = \begin{cases} \frac{1}{21}\left(\mathrm{Br} - 7C - \frac{21\Gamma}{40} + \frac{T_\xi}{16}\right) - \frac{(\chi+\kappa T_\xi)}{3}\left(\mathrm{Br} - 15C - 5\frac{\Gamma}{8} + \frac{T_\xi}{16}\right) & \text{for } k=0 \\ \frac{1}{8}\left(\mathrm{Br} - 4C - \frac{\Gamma}{3} + \frac{T_\xi}{16}\right) - \frac{(\chi+\kappa T_\xi)}{6}\left(\mathrm{Br} - 6C - 3\frac{\Gamma}{8} + \frac{T_\xi}{16}\right) & \text{for } k=1 \end{cases} \tag{21}$$

Note that well-known results for Poiseuille number for macrochannel ($\mathrm{Po} = 96.0$) and macrotube ($\mathrm{Po} = 64.0$), and fully developed Nusselt number for macrochannel ($\mathrm{Nu}_\infty = 8.325$) and macrotube ($\mathrm{Nu}_\infty = 4.364$) can be recovered with the current results. Present solution also recovers the result of van Rij et al. [30] for slit-channel as $\mathrm{Po} = 61.287$ and $\mathrm{Nu}_\infty = 5.549$ for the indicated input parameters in [30] ($a_1 = 1.0$, $a_2 = 1.125$, $a_3 = 0$, $b_1 = 1.667$, $b_2 = 3.012$, $\mathrm{Kn} = 0.04$, $\mathrm{Br} = 0$).

3 Results and Discussion

In this study, fully developed velocity profile, the fully developed temperature profile, and the associated Po and Nu are derived. Two second-order slip models, M1 and M2, are implemented to include the rarefaction effects and thermal creep. The viscous dissipation and the axial conduction are also included in the analysis. Coefficient b_1 is taken as 1.667, and γ is taken as 1.4 and Prandtl number is taken as 0.7 in the calculation of coefficient b_2, which are typical values for air being the working fluid in many engineering problems. In the calculation of a_1 and a_2, F_M is taken as unity, since it is the case for most of the air–solid couples used in engineering applications [6]. Although, Kn number is between 0.01 and 0.1 for slip-flow regime, in this study Kn is taken between 0 and 0.2 to see the effect of the thermal creep at the higher Kn numbers. As discussed earlier, some studies [2,3,8] indicated the validity of the Navier–Stokes equations with second-order models up to $\mathrm{Kn} \approx 0.25$. Present study considers the fully developed velocity and fully developed temperature. The hydrodynamic entrance length is proportional with Re (for macrochannels $\sim 0.1\,\mathrm{Re}R$), and the thermal entrance length is proportional with the Pe (for macrochannels $\sim 0.1\,\mathrm{Pe}R$) [32], which makes hydrodynamic and thermal entrance length of a microchannel flow typically short compared with the overall length. Therefore, analysis of the fully developed region holds for the many practical microchannel applications.

Using the closed form solutions derived in this study, one can predict the velocity and temperature profile. However, in this section only the results associated with the Poiseuille and Nusselt number, which are the main concerns of the design engineers, are presented. Moreover, choking phenomena occurred for negative

[2]The coefficients of the ξ term and $1/\mathrm{Pe}^2$ slightly differ from that of Ref. [31] due to the nondimensionlization of the velocity with u_o instead of u_mean.

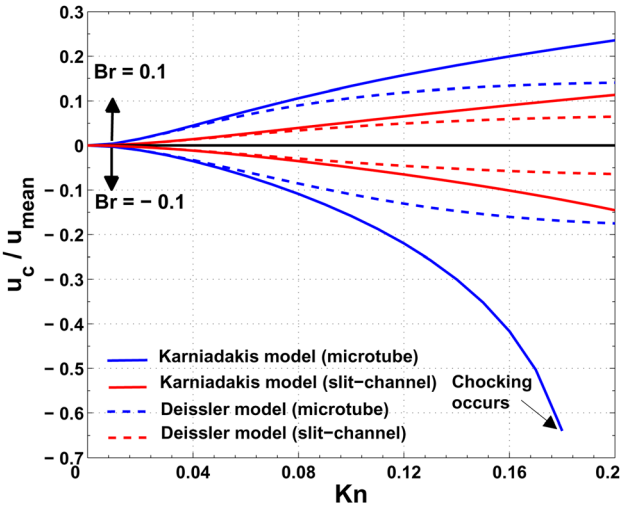

Fig. 1 Creep velocity over mean velocity for different Kn

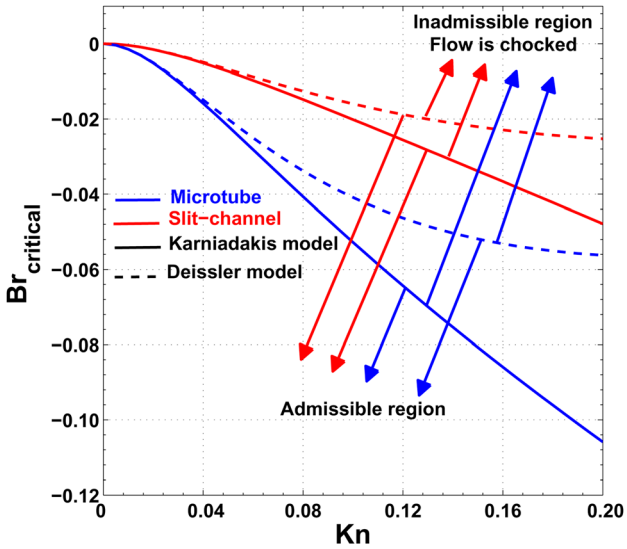

Fig. 2 Critical Br for different Kn

Br numbers is also discussed (a MATLAB script for the determination of the velocity and temperature profile, wall temperature variation, Poiseuille and Nusselt numbers with different slip models is given in Appendix).

Br number indicates the relative importance of the heating of the fluid due to viscous dissipation to the wall heating. For gaseous flow in a microchannel, order of magnitude estimates for some parameters can be summarized as $O(\mu) \sim 10^{-5}$ Ns/m^2, $O(U_o) \sim 1 - 10^{-3}$ m/s, $O(D_h) \sim 10^{-6} - 10^{-4}$ m and $O(|\dot{q}''|) \sim 1 - 10^3$ W/m^2. With these values, $O(|\mathrm{Br}|) \sim 10^1 - 10^{-8}$. $\mathrm{Br} > 0$ means fluid is being heated, and $\mathrm{Br} < 0$ means fluid is being cooled. With the inclusion of the thermal creep, temperature gradient at the channel wall assists the fluid flow for the fluid being heated. However, temperature gradient at the channel wall resists the fluid flow for the fluid being cooled. Figure 1 demonstrates the slip velocity at the wall due to the thermal creep over the mean velocity for both microtube and microchannel. M1 predicts higher creep velocity than that of M2 for both geometries. For negative Br, thermal creep resists the fluid flow. Therefore, flow can be stopped (i.e., choked) by the reverse flow induced by the thermal creep. Chocking occurs when the square root term in Eq. (12) is less than and equal to zero. As seen form the figure, M1 predicts a choking Kn value close to 0.18. On the other hand, M2 does not predict any chocking for the range of Kn used in this study.

Actually, for negative Br there exists a Br (< 0) value for which the flow is chocked for a given Kn. Figure 2 shows the critical Br for different Kn for both models. As Kn increases, in order to have unchocked flow, higher Br in magnitude is needed. For a given u_o and channel size, decreased |Br| means higher cooling rate. If the cooling rate is too high, the resulting temperature gradient at the wall introduces a high enough thermal creep to chock the flow. As illustrated, M2 predicts a wider admissible region than that of M1.

The fully developed velocity profile and Po number are function of only Kn for the case without thermal creep, and function of Kn and Br for the case with thermal creep. Figure 3 shows the normalized Po both for microtube and slit-channel as a function of Kn and Br. First-order slip model is also included in the figure. With the increasing Kn, slip velocity at the wall increases which means a reduced shear stress at the wall. As the shear stress decreases, so does the Po which means that rarefaction effect has a reduced pressure drop effect for a given volumetric flow rate. Since M1 indicates lower slip velocity and M2 indicates higher slip velocity than that of first-order model, former predicts higher and latter predicts lower Po than that of first-order model. As expected, the deviation between the first-order model and the second-order models increases as Kn increases. For $\mathrm{Br} > 0$, thermal creep assists the fluid flow. Therefore, with the inclusion of the thermal creep, Po decreases for both models and Po further decreases, and for $\mathrm{Br} < 0$, thermal creep resists the fluid flow, and Po increases. As seen from the figure, inclusion of the thermal creep has an appreciable effect on Po. Po values for both geometries are tabulated in Tables 2 and 3.

Fully developed temperature is function of Kn, Br, Pe, and thermal creep. On the other hand, the fully developed Nu is function of same parameters except the Pe, which means Pe number only affects the local Nu in the thermal entrance region. Fully developed Nu values for $\mathrm{Br} = 0$ are tabulated for both geometries in Tables 4 and 5. The results of Cetin et al. [18] and of first-order slip model are also included in Tables 4 and 5, respectively, for comparison (since the figure form of these data would be too crowded, only the tabulated data are given here). Fully developed Nu values for different Br other than zero are tabulated in Tables 6 and 7. For the constant wall heat flux thermal boundary condition, Nu is the indication of the temperature difference between the wall temperature and the mean temperature. Higher the Nu, smaller the temperature difference between the wall and mean which is desired for thermal systems.

For the case without thermal creep (i.e., $\mathrm{Br} = 0$), story for Nu is different for microtube and slit-channel. Moving from a first-order model to a second-order model has two combined effects on Nu. First, slip velocity at the wall changes which would affect the mean velocity. Second, the wall temperature changes. M1 predicts higher wall temperature and lower slip velocity than that of first-order model. As a combined effect, M1 predicts lower Nu for microtube and higher Nu for slit-channel compared with first-order model. However, M2 predicts higher wall temperature and higher slip velocity than that of first-order model. As a combined effect, M2 predicts higher Nu for small Kn and lower Nu for higher Kn for microtube, and lower Nu for all Kn for slit-channel compared with first-order model. Deviation between the first-order model and the second-order model increases as Kn increases for both models which indicate the necessity of second-order model as rarefaction increases.

The slip velocity at the wall has an effect on the heat transfer through affecting the convection at the wall. Slip velocity over the mean velocity values is tabulated in Tables 8 and 9. For $\mathrm{Br} > 0$, thermal creep assists the flow and increases the convection at the channel wall; therefore, the slip velocity increases for both models, including the thermal creep for both geometries. The same trend is valid for Nu also. The higher the convection at the wall, the higher the Nu. Except at high Kn for slit-channel, M2 model

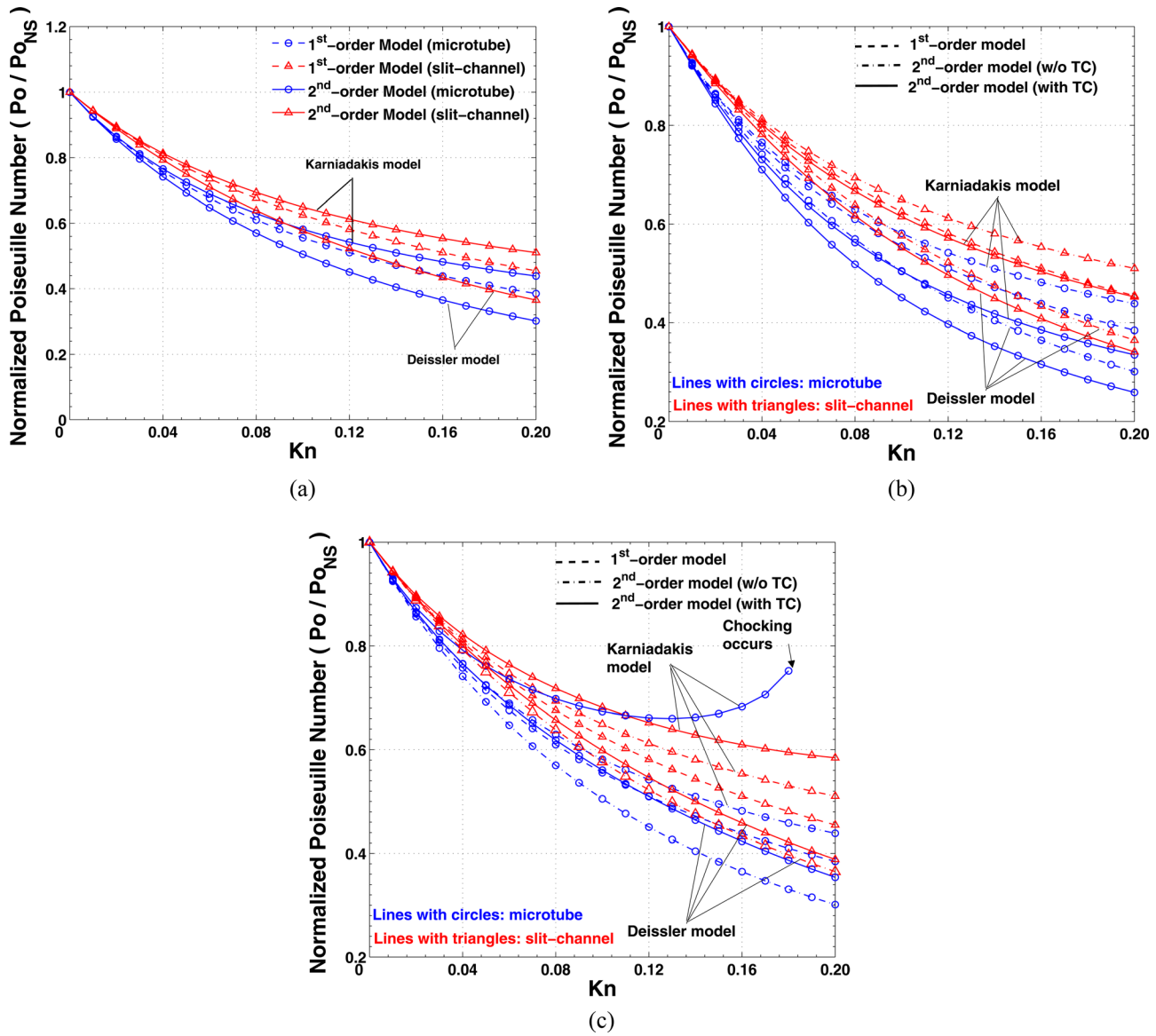

Fig. 3 Variation of the Po as a function of Kn (*a*) Br = 0, (*b*) Br = 0.1, and (c) Br = −0.1

predicts lower Nu than that of first-order model, and the inclusion of the thermal creep predicts even lower Nu. Note that M1 without thermal creep predicts lower slip at the wall, and with the inclusion of the thermal creep M1 predicts slip at the wall very close to that of first-order model, which also results in Nu close to again that of first-order model.

For $Br < 0$, thermal creep resists the flow and decreases the convection at the wall; hence, the slip velocity decreases for both models, including the thermal creep for both geometries. The same trend can be also observed for Nu. The lower the convection at the wall, the lower the Nu. Except at high Kn, M2 model predicts higher Nu compared with the case without the thermal creep.

Table 2 Po values for different models and for different Kn and Br (slit-channel)

		Second-order model [6]			Second-order model [7]		
Kn	First-order model	w/o TC	with TC	with TC	w/o TC	with TC	with TC
0.0	96.0	96.0	96.0	96.0	96.0	96.0	96.0
0.04	77.4	78.0	76.9	78.9	76.1	75.1	76.9
0.08	64.9	66.6	64.0	68.9	61.3	59.2	63.1
0.12	55.8	58.8	54.9	62.6	50.1	47.7	52.4
0.16	49.0	53.1	48.3	58.5	41.6	39.2	44.0
0.20	43.6	49.0	43.4	56.1	35.0	32.8	37.3
			Br = 0.1	Br = −0.1		Br = 0.1	Br = −0.1

Table 3 Po values for different models and for different Kn and Br (microtube)

		Second-order model [6]			Second-order model [7]		
Kn	First-order model	w/o TC	with TC	with TC	w/o TC	with TC	with TC
0.0	64.0	64.0	64.0	64.0	64.0	64.0	64.0
0.04	48.5	49.0	46.8	50.7	47.4	45.4	49.0
0.08	39.0	40.3	36.0	44.7	36.5	33.2	39.6
0.12	32.7	34.7	29.2	42.3	28.8	25.4	32.6
0.16	28.1	30.8	24.7	43.7	23.4	20.2	27.1
0.20	24.6	28.1	21.5	—	19.3	16.6	22.6
			Br = 0.1	Br = −0.1		Br = 0.1	Br = −0.1

Table 4 Comparison of the Nu_∞ for slit-channel (Br = 0)

	First-order		Second-order [6]		Second-order [7]	
Kn	Present	Ref. [17]	w/o TC	with TC	w/o TC	with TC
0.0	8.235	8.235	8.235	8.235	8.235	8.235
0.04	6.819	6.819	6.819	—	6.799	—
0.08	5.724	5.724	5.754	—	5.549	—
0.12	4.894	—	4.978	—	4.489	—
0.16	4.256	—	4.404	—	3.627	—
0.20	3.757	—	3.969	—	2.947	—

Table 5 Comparison of the Nu_∞ for microtube (Br = 0)

	First-order		Second-order [6]		Second-order [7]	
Kn	Present	Ref. [17]	w/o TC	with TC	w/o TC	with TC
0.0	4.364	4.364	4.364	4.364	4.364	—
0.04	3.749	3.749	3.717	—	3.842	—
0.08	3.155	3.155	3.107	—	3.255	—
0.12	2.681	—	2.643	—	2.664	—
0.16	2.313	—	2.298	—	2.143	—
0.20	2.026	—	2.038	—	1.721	—

Table 6 Nu_∞ values for different Kn and Br for slit-channel

		Second-order [6]		Second-order [7]		
Kn	First-order model	w/o TC	with TC	w/o TC	with TC	Br
0.0	7.692	7.692	7.692	7.692	7.692	
0.04	6.480	6.457	6.480	6.540	6.559	
0.08	5.500	5.468	5.510	5.545	5.559	
0.12	4.739	4.720	4.771	4.659	4.655	0.1
0.16	4.144	4.151	4.210	3.895	3.877	
0.20	3.672	3.711	3.766	3.256	3.232	
0.0	8.861	8.861	8.861	8.861	8.861	
0.04	7.195	7.222	7.204	7.079	7.065	
0.08	5.966	6.072	6.036	5.554	5.543	
0.12	5.059	5.266	5.217	4.330	4.332	−0.1
0.16	4.375	4.690	4.625	3.394	3.404	
0.20	3.846	4.266	4.183	2.692	2.704	

Table 7 Nu_∞ values for different Kn and Br for microtube

		Second-order [6]		Second-order [7]		
Kn	First-order model	w/o TC	with TC	w/o TC	with TC	Br
0.0	3.934	3.934	3.934	3.934	3.934	
0.04	3.485	3.433	3.490	3.657	3.703	
0.08	2.990	2.885	2.972	3.335	3.353	
0.12	2.572	2.442	2.536	2.942	2.901	0.1
0.16	2.238	2.102	2.200	2.526	2.449	
0.20	1.971	1.839	1.941	2.136	2.049	
0.0	4.898	4.898	4.898	4.898	4.898	
0.04	4.056	4.052	4.001	4.047	4.015	
0.08	3.340	3.367	3.283	3.178	3.164	
0.12	2.800	2.880	2.758	2.434	2.452	−0.1
0.16	2.394	2.535	2.345	1.861	1.895	
0.20	2.084	2.284	—	1.441	1.475	

Although in these results, Br and Kn vary independent of each other, in many engineering applications regarding microchannels, this is not the case. In the engineering application with microchannels, the devices typically operate at the vicinity of the atmospheric conditions, which means that increase in the Kn indicates the reduction in the size of the channel. Br has also size dependence. Therefore, depending on the limits of the mass flow rate, keeping Br or Kn constant and the variation of remaining one independently is not actually something practical.

Table 8 Slip velocity over the mean velocity for different Kn and Br for slit-channel

		Second-order [6]		Second-order [7]		
Kn	First-order model	w/o TC	with TC	w/o TC	with TC	Br
0.0	0	0	0	0	0	
0.04	0.19	0.19	0.19	0.21	0.22	
0.08	0.32	0.31	0.33	0.36	0.38	
0.12	0.42	0.39	0.43	0.48	0.50	0.1
0.16	0.49	0.45	0.50	0.57	0.60	
0.20	0.55	0.49	0.55	0.64	0.66	
0.0	0	0	0	0	0	
0.04	0.19	0.19	0.18	0.21	0.19	
0.08	0.32	0.31	0.28	0.36	0.34	
0.12	0.42	0.39	0.35	0.48	0.45	−0.1
0.16	0.49	0.45	0.39	0.57	0.54	
0.20	0.55	0.49	0.42	0.64	0.61	

Table 9 Slip velocity over the mean velocity for different Kn and Br for microtube

		Second-order [6]		Second-order [7]		
Kn	First-order model	w/o TC	with TC	w/o TC	with TC	Br
0.0	0	0	0	0	0	
0.04	0.24	0.24	0.27	0.26	0.29	
0.08	0.39	0.37	0.44	0.43	0.48	
0.12	0.49	0.46	0.54	0.55	0.60	0.1
0.16	0.56	0.52	0.61	0.64	0.68	
0.20	0.62	0.56	0.66	0.70	0.74	
0.0	0	0	0	0	0	
0.04	0.24	0.24	0.21	0.26	0.23	
0.08	0.39	0.37	0.30	0.43	0.38	
0.12	0.49	0.46	0.34	0.55	0.49	−0.1
0.16	0.56	0.52	0.32	0.64	0.57	
0.20	0.62	0.56	—	0.70	0.65	

4 Summary and Outlook

In this study, the velocity profile, the temperature profile, and the corresponding Po and Nu numbers are determined for a fully developed gaseous flow in a 2D microchannel (i.e., both microtube and slit-channel) with a constant wall heat flux thermal boundary condition. Neat, closed form solutions for the fully developed velocity profile, temperature profile, Po and Nu number are derived analytically. Two different slip models (M1 and M2) together with the thermal creep are included in the analysis. The effect of the thermal creep on Po and Nu is discussed. A MATLAB script that computes the fully developed velocity profile (as a function of nondimensional axial coordinate), temperature profile (as a function of nondimensional radial and axial coordinate), wall temperature (as a function of nondimensional axial coordinate), and the corresponding Po and Nu number values with different Kn, Br, Pe, and second-order models are given in Appendix. Despite the fact that the present study has some limitations (such as incompressible flow, fully developed conditions), the author believes that with this closed form solution, the fundamental physical mechanism that affects the heat transfer characteristics for microchannel flows could be explored.

Deviation from both the continuum behavior and from the first-order model is observed. It is also observed that different second-order models predict different results for the flow field and temperature field. The verification of the current results with the experimental results to see the most suitable second-order model would be problematic. The deviation of the second-order models from the continuum in terms of Po and Nu is relatively small which would most probably be within the uncertainty of the experimental results. However, solutions derived using kinetic theory for the given problem can supply some insight to validate the second-order models. The exploration of the effect of the thermal creep in the thermally developing region and the comparison of the Navier–Stokes solution with the kinetic theory solutions will be the future research directions.

Nomenclature

a_1 = coefficient defined in Eq. (1)
a_2 = coefficient defined in Eq. (1)
a_3 = coefficient defined in Eq. (1)
b_1 = coefficient defined in Eq. (2)
b_2 = coefficient defined in Eq. (2)
Br = Brinkman number
D = tube diameter
H = slit-channel half height
D_h = hydraulic diameter
k = thermal conductivity
Kn = Knudsen number
Nu = Nusselt number
P = pressure
Pe = Peclet number ($u_o D_h/\alpha$)
$\dot{q}''$ = wall heat flux
Re = Reynolds number ($\rho u_{mean} D_h/\mu$)
R = tube radius
T = temperature
T_i = inlet temperature
T_w = wall temperature
u = x-velocity
u_c = creep velocity (κT_ξ)
u_o = reference velocity
u_w = wall x-velocity
x = longitudinal coordinate
α = thermal diffusivity
Γ = parameter used in Eq. (13)
η = nondimensional radial coordinate
θ = nondimensional temperature
θ_m = nondimensional mean temperature
θ_w = nondimensional wall temperature
θ_∞ = nondimensional fully developed temperature
κ = parameter defined in Eq. (7)
λ = mean-free-path
μ = viscosity
ξ = nondimensional longitudinal coordinate
Υ = parameter defined in Eq. (21)
ϕ = nondimensional temperature
χ = parameter defined in Eq. (7)
Ω = parameter defined in Eq. (9)

Appendix: MATLAB Script

```
clear all; clc;
syms ksi eta

F_T = 1;
Gamma = 1.4;
Pr = 0.7;
Kn = 0.08;
Br = -0.1;
Pe = 0.5;
a1 = 1;
b1 = (2-F_T)/F_T*2*Gamma/(Gamma+1)/Pr;

%&&&&&&&&&&&&&&&&&&&&&&&&&
k = 0;
%***********************
% 0 -> slit-channel
% 1 -> microtube
%***********************

%&&&&&&&&&&&&&&&&&&&&&&&&&
model = 1;
%***********************
% 1 -> First-order model
% 2 -> Karniadakis model
% 3 -> Deissler model
%***********************
switch model
case 1% First-order model
   a2 = 0;
   b2 = 0;
case 2% Karniadakis model
   a2 = 1/2;
   b2 = b1/2;
case 3% Deissler model
   a2 = -9/8;
   b2 = -9/128*(177*Gamma-145)/(Gamma+1);
end
%&&&&&&&&&&&&&&&&&&&&&&&&&

%&&&&&&&&&&&&&&&&&&&&&&&&&
TC = 0;
%***********************
% 0 -> no thermal creep
% 1 -> thermal creep
%***********************
switch TC
case 0
   a3_tilda = 0;
case 1
   a3_tilda = 3/2*(1-k)/pi*(Gamma-1)/Gamma;
end
%&&&&&&&&&&&&&&&&&&&&&&&&&
X = 1+4*a1*Kn-8*a2*Kn^2;
%&&&&&&&&&&&&&&&&&&&&&&&&&&&&&&&&&
if Br == 0||Kn == 0||a3_tilda == 0
beta = 1-(3-k)*X;
Tx = -2*(2+k)*(2*(2-k)*Br+3-2*k)/beta;
K = 0;
else
K = a3_tilda*Kn^2/Br;
beta = 1-(3-k)*X;
Tx = (beta+sqrt(beta^2+16*(3+k)*K*...
(2*(2-k)*Br+3-2*k)))/(2*(3-k)*K);
end
%&&&&&&&&&&&&&&&&&&&&&&&&&&&&&&&&

%&&&&&&&&&&&&&&&&&&&&&&&&&&&&&&&&
Um_over_Uo = X-1/(3-k)+K*Tx;
Ome = 1/Um_over_Uo;
Po = 16*2*(2-k)*Ome;
%&&&&&&&&&&&&&&&&&&&&&&&&&&&&&&&&
G = Tx*(X+K*Tx);
%&&&&&&&&&&&&&&&&&&&&&&&&&&&&&&&&
switch k
case 0
C = 1/15*(Br+Tx/16)-G/24+...
   Ome/3*(12*Tx/Pe^2-8*Br/105+G/30-Tx/210);
case 1
C = 1/6*(Br+Tx/16)-G/16+...
   Ome/3*(6*Tx/Pe^2-Br/8+G/32-Tx/128);
end
%&&&&&&&&&&&&&&&&&&&&&&&&&&&&&&&&

%&&&&&&&&&&&&&&&&&&&&&&&&&&&&&&&&
T_inf = Tx*ksi+G/8*eta^2-...
```

```
        (Br+Tx/16)*eta4/(3-k)+C
T_wall=subs(T_inf,eta,1)+...
        2*b1*Kn-4*b2*Kn2*...
        subs(diff(diff(T_inf,eta),eta),eta,1)
ubar=X-eta2+K*Tx;
T_mean=2k*Ome*...
        int(ubar*T_inf*etak,eta,0,1)
Nu=-2(2-k)/...
     (subs(T_mean,ksi,0)-subs(T_wall,ksi,0))
%&&&&&&&&&&&&&&&&&&&&&&&&&&&&&&&&
```

References

[1] Yaman, M., Khudiyev, T., Ozgur, E., Kanik, M., Aktas, O., Ozgur, E. O., Deniz, H., Korkut, E., and Bayindir, M., 2011, "Arrays of Indefinitely Long Uniform Nanowires and Nanotubes," Nature Mater., **10**(7), pp. 494–501.

[2] Colin, S., 2004, "Validation of a Second-Order Slip Flow Model in Rectangular Microchannels," Heat Transfer Eng., **25**(3), pp. 23–30.

[3] Colin, S., 2005, "Rarefaction and Compressibility Effects on Steady and Transient Gas Flows in Microchannels," Microfluid. Nanofluid., **1**, pp. 268–279.

[4] Weng, H. C., 2010. "Laminar, Transitional and Turbulent Friction Factors for Gas Flows in Smooth and Rough Microtubes," Int. J. Therm. Sci., **49**, pp. 248–255.

[5] Yang, Y., Morini, G. L., Lorenzini, M., Hong, C., Asako, Y., and Brandner, J. J., 2012, "Transitional and Turbulent Convective Heat Transfer compressible Gas Flows Through Microtubes," Proceedings of the ASME 2012 10th International Conference on Nanochannles, Microchannels and Minichannels, ICNMM2012, Puerto Rico, USA, Paper No. 73261, July 8–12.

[6] Karniadakis, G. E., Beskok, A., and Aluru, N., 2005, *Microflows and Nanoflows: Fundamentals and Simulations*, Springer, New York, pp. 51–74, 167–172.

[7] Deissler, R. G., 1964, "An Analysis of Second-Order Slip Flow and Temperature-Jump Boundary Conditions for Rarefied Gases," Int. J. Heat Mass Transfer, **7**, pp. 681–694.

[8] Duan, Z., 2012, "Second-Order Gaseous Slip Flow Models in Long Circular and Noncircular Microchannels and Nanochannels," Microfluid. Nanofluid., **12**, pp. 805–820.

[9] Weng, H. C., and Chen, C.-K., 2008, "A Challenge in Navier–Stokes Based Continuum Modeling: Maxwell–Burnett Slip Law," Phys. Fluids, **20**, p. 106101.

[10] Cetin, B., Yazicioglu, A., and Kakac, S., 2008, "Fluid Flow in Microtubes With Axial Conduction Including Rarefaction and Viscous Dissipation," Int. Commun. Heat Mass Transfer, **35**, pp. 535–544.

[11] Aubert, C., and Colin, S., 2001, "High-Order Boundary Conditions for Gaseous Flows in Rectangular Microducts," Microscale Thermophys. Eng., **5**, pp. 41–54.

[12] Niazmand, H., Amiri-Jaghargh, A., and Renksizbulut, M., 2010, "Slip-Flow and Heat Transfer in Isoflux Rectangular Microchannels With Thermal Creep Effects," J. Appl. Fluid Mech., **3**(2), pp. 33–41, Available at www.jafmonline.net

[13] Amiri-Jaghargh, A., Niazmand, H., and Renksizbulut, M., 2010, "Cooling in a Constant Wall Temperature Microchannels With Thermal Creep Effects," Proceedings of the ASME 8th International Conference on Nanochannles, Microchannels and Minichannels, ICNMM2010, Montreal, Canada, Paper No. 30770, August 1–5.

[14] Ameel, T. A., Barron, R. F., Wang, X. M., and Warrington, R. O., 1997, "Laminar Forced Convection in a Circular Tube With Constant Heat Flux and Slip Flow," Microscale Thermophys. Eng., **1**, pp. 303–320.

[15] Chen, C. S., and Kuo, W. J., 2004, "Heat Transfer Characteristics of Gaseous Flow in Long Mini- and Microtubes," Numer. Heat Transfer, Part A, **46**(5), pp. 497–514.

[16] Aydin, O., and Avci, M., 2006, "Analysis of Micro-Graetz Problem in a Microtube," Nanoscale Microscale Thermophys. Eng., **10**(4), pp. 345–358.

[17] Cetin, B., Yazicioglu, A., and Kakac, S., 2009, "Slip-Flow Heat Transfer in Microtubes With Axial Conduction and Viscous Dissipation—An Extended Graetz Problem," Int. J. Therm. Sci., **48**, pp. 1673–1678.

[18] Çetin, B., Yuncu, H., and Kakac, S., 2006, "Gaseous Flow in Microchannels With Viscous Dissipation," Int. J. Transp. Phenom., **8**, pp. 297–315.

[19] Xiao, N., Elsnab, J., and Ameel, T., 2009, "Microtube Gas Flows With Second-Order Slip Flow and Temperature Jump Boundary Conditions," Int. J. Therm. Sci., **48**(2), pp. 243–251.

[20] Cetin, B., and Bayer, O., 2011, "Evaluation of Nusselt Number for a Flow in a Microtube Using Second-Order Slip Model," Therm. Sci., **15**(Suppl. 1), pp. 103–109.

[21] Cetin, B., 2012, "Evaluation of Nusselt Number for a Flow in a Microtube With Second-Order Model Including Thermal Creep," Proceedings of the ASME 10th International Conference on Nanochannles, Microchannels and Minichannels, ICNMM2012, Puerto Rico, USA, Paper No. 73321, July 8–12.

[22] Xue, H., Ji, H., and Shu, C., 2003, "Prediction of Flow and Heat Transfer Characteristics in Micro-Couette Flow," Microscale Thermophys. Eng., **7**(1), pp. 51–68.

[23] Jeong, H. E., and Jeong, J. T., 2006, "Extended Graetz Problem Including Streamwise Conduction and Viscous Dissipation in Microchannels," Int. J. Heat Mass Transfer, **49**, pp. 2151–2157.

[24] Roy, S., and Chakraborty, S., 2007, "Near-Wall Effects in Micro Scale Couette Flow and Heat Transfer in the Maxwell-Slip Regime," Microfluid. Nanofluid., **3**(4), pp. 437–449.

[25] Niazmand, H., and Rahimi, B., 2010, "High Order Slip and Thermal Creep Effects in Micro Channel Natural Convection," Proceedings of the ASME 8th International Conference on Nanochannles, Microchannels and Minichannels, ICNMM2010, Montreal, Canada, Paper No. 30688, August 1–5.

[26] Weng, H. C., and Chen, C.-K., 2008, "On the Importance of Thermal Creep in Natural Convection Gas Microflow With Wall Heat Fluxes," J. Phys. D: Appl. Phys., **41**, p. 115501.

[27] van Rij, J., Ameel, T., and Harman, T., 2009, "An Evaluation of Secondary Effects on Microchannel Frictional and Convective Heat Transfer Characteristics," Int. J. Heat Mass Transfer, **52**, pp. 2792–2801.

[28] Duan, Z., and Muzychka, Y. S., 2008, "Slip Flow Heat Transfer in Annular Microchannels With Constant Heat Flux," ASME J. Heat Transfer, **130**, p. 092401.

[29] Aziz, A., and Niedbalski, N., 2011, "Thermally Developing Microtube Gas Flow With Axial Conduction and Viscous Dissipation," Int. J. Therm. Sci., **50**, pp. 332–340.

[30] van Rij, J., Harman, T., and Ameel, T., 2007, "The Effect of Creep Flow on Two-Dimensional Isoflux Microchannels," Int. J. Therm. Sci., **46**, pp. 1095–1103.

[31] Vick, B., and Ozisik, M. N., 1981, "An Exact Analysis of Low Peclet Number Heat Transfer in Laminar Flow With Axial Conduction," Lett. Heat Mass Transfer, **8**, pp. 1–10.

[32] Incropera, F. P., and DeWitt, D. P., 1996, *Fundamentals of Heat and Mass Transfer*, 4th ed., John Wiley & Sons, New York, p. 426.

[33] Weng, H. C., 2010, "Second-Order Slip Flow and Heat Transfer in a Microchannel," Comput. Commun. Control Autom. (3CA), **2**, pp. 13–16.